Shift of Intracellular Chloride Concentration in Ganglion and Amacrine Cells of Developing Mouse Retina

Ling-Li Zhang, Hemal R. Pathak, Douglas A. Coulter, Michael A. Freed and Noga Vardi

J Neurophysiol 95:2404-2416, 2006. First published Dec 21, 2005; doi:10.1152/jn.00578.2005

J Neurophysiol 95: 2404–2416, 2006.
First published December 21, 2005; doi:10.1152/jn.00578.2005.

Shift of Intracellular Chloride Concentration in Ganglion and Amacrine Cells of Developing Mouse Retina

Ling-Li Zhang,[1] Hemal R. Pathak,[1] Douglas A. Coulter,[1,2] Michael A. Freed,[1] and Noga Vardi[1]
[1]*Department of Neuroscience, University of Pennsylvania School of Medicine; and* [2]*Division of Neurology, Pediatric Regional Epilepsy Program, Children's Hospital of Philadelphia, Philadelphia, Pennsylvania*

Submitted 3 June 2005; accepted in final form 19 December 2005

Zhang, Ling-Li, Hemal R. Pathak, Douglas A. Coulter, Michael A. Freed, and Noga Vardi. Shift of intracellular chloride concentration in ganglion and amacrine cells of developing mouse retina. *J Neurophysiol* 95: 2404–2416, 2006. First published December 21, 2005; doi:10.1152/jn.00578.2005. GABA and glycine provide excitatory action during early development: they depolarize neurons and increase intracellular calcium concentration. As neurons mature, GABA and glycine become inhibitory. This switch from excitation to inhibition is thought to result from a shift of intracellular chloride concentration ($[Cl^-]_i$) from high to low, but in retina, measurements of $[Cl^-]_i$ or chloride equilibrium potential (E_{Cl}) during development have not been made. Using the developing mouse retina, we systematically measured $[Cl^-]_i$ in parallel with GABA's actions on calcium and chloride. In ganglion and amacrine cells, fura-2 imaging showed that before postnatal day (P) 6, exogenous GABA, acting via ionotropic GABA receptors, evoked calcium rise, which persisted in HCO_3^-- free buffer but was blocked with 0 extracellular calcium. After P6, GABA switched to inhibiting spontaneous calcium transients. Concomitant with this switch we observed the following: 6-methoxy-*N*-ethylquinolinium iodide (MEQ) chloride imaging showed that GABA caused an efflux of chloride before P6 and an influx afterward; gramicidin-perforated-patch recordings showed that the reversal potential for GABA decreased from −45 mV, near threshold for voltage-activated calcium channel, to −60 mV, near resting potential; MEQ imaging showed that $[Cl^-]_i$ shifted steeply around P6 from 29 to 14 mM, corresponding to a decline of E_{Cl} from −39 to −58 mV. We also show that GABAergic amacrine cells became stratified by P4, potentially allowing GABA's excitatory action to shape circuit connectivity. Our results support the hypothesis that a shift from high $[Cl^-]_i$ to low causes GABA to switch from excitatory to inhibitory.

INTRODUCTION

To develop normally, brain circuits, including retina, require neural activity. In early neuronal development, before the major excitatory transmitter glutamate is released, the main source of excitation is provided by GABA and glycine (Ben Ari 2001, 2002). GABA depolarizes neurons, activates voltage-gated calcium channels, and increases intracellular calcium concentration ($[Ca^{2+}]_i$) (Leinekugel et al. 1995; Owens et al. 1996; Yuste and Katz 1991). Through depolarization and calcium elevation, GABA regulates differentiation, survival, dendritic mobility, and spontaneous activity (Fischer et al. 1998; Liu et al. 1997; Marty et al. 1996; Redburn 1992; Wong and Wong 2001; Young and Cepko 2004). In retina, GABA and glycine also modulate retinal waves, spontaneous bursts of action potentials that propagate across amacrine and ganglion cells and are critical for refinement of the retinotopic and eye-specific maps in the brain (Firth et al. 2005; Penn et al. 1998; Shatz and Stryker 1988). GABA and glycine affect waves differently in different species: they increase the frequency of calcium transients (ferret: Fischer et al. 1998), control wave propagation rate (turtle: Sernagor et al. 2003), or generate the waves (rabbit: Zheng et al. 2004; Zhou 2001).

The excitatory action of GABA is mediated by the ionotropic GABA receptor, which permeates primarily chloride but may also permeate bicarbonate. Therefore depolarization by GABA may be due to efflux of chloride if the chloride equilibrium potential (E_{Cl}) is above the resting membrane potential (E_{rest}) or to efflux of HCO_3^-, the typical reversal potential of which is 0 mV (Bormann et al. 1987; Kaila et al. 1989). In several brain regions, GABA's depolarizing effect correlates with measurements of E_{Cl}, lending support to the chloride hypothesis (Ehrlich et al. 1999; Eilers et al. 2001; Owens et al. 1996; Yamada et al. 2004). However, in retina, neither hypothesis was tested, and the evidence supporting the chloride hypothesis remained indirect.

In rat retina, the chloride extruder, KCC2, is undetectable early in development and becomes significantly greater at about the stage when GABA was predicted to switch from excitatory to inhibitory (Vu et al. 2000). This has been interpreted to mean that $[Cl^-]_i$ is initially high and declines as the extruder appears. This interpretation, however reasonable, needed testing with actual measurements of the developmental changes in $[Cl^-]_i$, E_{Cl}, and the reversal potential of GABA (E_{GABA})—all in the same species, and only then comparing them to the appearance of KCC2. These measurements carry additional importance because the molecular mechanisms of chloride's accumulation in early development remain to be established in any brain region and to do so requires firm quantification of these various parameters. We performed these measurements in mouse where the availability of gene knockouts will facilitate studying the molecular mechanisms. Here we show, by optical measurements of $[Cl^-]_i$ and $[Ca^{2+}]_i$ and electrical measurements of E_{Cl} with perforated-patch recordings, that from postnatal day (P) 0 to P6, $[Cl^-]_i$ is high enough for GABA to cause chloride efflux, calcium rise, and excitation. After P6, $[Cl^-]_i$ declines abruptly and GABA becomes inhibitory.

Address for reprint requests and other correspondence: N. Vardi, 123 Anatomy and Chemistry Bldg., University of Pennsylvania School of Medicine, Philadelphia, PA 19104-6058 (E-mail: noga@retina.anatomy.upenn.edu).

The costs of publication of this article were defrayed in part by the payment of page charges. The article must therefore be hereby marked "*advertisement*" in accordance with 18 U.S.C. Section 1734 solely to indicate this fact.

METHODS

Immunostaining

Newborn mice were deeply anesthetized on postnatal days P0–P6 with halothane and killed by decapitation. Older mice were killed with ketamine (85 μg/g) and xylazine (13 μg/g ip) followed by anesthetic overdose. Animals were treated in compliance with federal regulations and University of Pennsylvania policy. After enucleation, eye cups were immersion-fixed for 1 h at room temperature in 4% paraformaldehyde and 0.01% glutaraldehyde in 0.1 M phosphate buffer at pH 7.4 and cryoprotected overnight with 30% sucrose in phosphate buffer. Eyes were frozen in a mixture of tissue-freezing medium (Electron Microscopy Sciences, Ft. Washington, PA) and 20% sucrose (1:2) and cryosectioned vertically at 10 μm. Sections were preblocked, then stained by incubation in guinea pig anti-GABA (Chemicon, Temecula, CA) diluted with 0.1 M phosphate buffer containing 10% normal goat serum, 5% sucrose, and 0.3% Triton X-100 (overnight at 4°C). Sections were then washed, incubated in donkey anti-guinea pig IgG conjugated to FITC (3 h; Jackson Immunoresearch, West Grove, PA), washed, and mounted in Vectashield (Vector Laboratories, Burlingame, CA). Sections were visualized with a confocal microscope (Leica, Nussloch, Germany). At each age group, omitting the primary antibody gave no staining at all.

Calcium imaging

A retina was cleaned of vitreous, detached from the pigment epithelium, and cut into two to three pieces. Retinal pieces were mounted on a filter paper and maintained in bicarbonate-based Ames medium saturated with carbogen (95% O_2-5% CO_2). For bicarbonate-free Ames medium, $NaHCO_3$ was replaced with 20 mM HEPES, and the solution was saturated with oxygen (100% O_2). In mice >P7, ganglion cells were exposed by gently scratching the vitreal surface with a scalpel tip or a brush.

Retinal pieces were loaded in 5−10 μM fura-2 AM (Molecular Probes, Eugene, OR) in oxygenated Ames medium for 1 h at 27–30°C. A retina was placed in an optical recording chamber mounted on a fixed-stage, upright microscope (Olympus BX51WI), and continuously superfused (3–4 ml/min) with Ames medium preheated to 30–33°C. Fura-2 was alternately excited at 340 and 380 nm with a xenon arc lamp in lambda DG4 (Sutter Instrument, Novato, CA) and attenuated with a neutral density filter (0.25). Fluorescent images were viewed with a ×40 water-immersion lens (NA, 0.8, Olympus, Tokyo, Japan), filtered with a 510/40-nm emission filter (set 71000, Chroma, Rockingham, VT), and captured with Hamamatsu Orca ER digital CCD camera (Hamamatsu, Hamamatsu City, Japan). Wavelength switch and image capturing were controlled by Openlab software (Improvision, Lexington, MA) running under Mac G4. To minimize potential UV phototoxicity, the illuminated retinal area was restricted by closing the field aperture to match the CCD imaging field (250 × 190 μm), and pixels were binned (2 × 2). Exposure time was 25–200 ms, and sampling interval 3–4 s.

Chloride imaging

Fresh 6-methoxy-*N*-ethyl-1,2-dihydroquinoline (dihydro-MEQ) was synthesized from 5 mg 6-methoxy-*N*-ethylquinolinium iodide (MEQ) according to the protocol provided by Molecular Probe (Molecular Probes). The reduced product was resuspended in dimethyl sulfoxide and added to Ames medium to yield a loading concentration of ~300 μM dihydro-MEQ. Retinal pieces, prepared as described in the preceding text, were incubated in oxygenated dihydro-MEQ for 1 h at 27–30°C. To identify cells and monitor their volume, 1 μM calcein and 0.001- 0.02% pluronic acid were added for the last 15 min of loading. For dual calcium and chloride imaging, the loading solution contained 10 μM calcium indicator, Calcium Green-1 AM, and 0.001–0.02% pluronic acid. During loading, intracellular oxidation converted the membrane-permeable dihydro-MEQ into the charged and impermeable MEQ. After loading, retinas were transferred into fresh Ames medium at room temperature and then transferred to the recording chamber. The chamber was maintained at 27–29°C (rather than 33°C) to reduce MEQ leakage and increase MEQ sensitivity (Fukuda et al. 1998). The optical setup and acquisition system was the same as for calcium imaging except that excitation and emission was filtered for MEQ and calcein or for MEQ and Calcium Green-1 fluorescence. Excitation alternated between 345 nm (D345/10×, Chroma) and 485 nm (S485/25×, Chroma), and emission was collected with a dual band filter with peaks at 450 and 535 nm (set 91018, Chroma). Images were collected every 10–15 s to determine intracellular chloride, and every 3–4 s to record GABA-evoked chloride changes.

Optical signal analysis

Imaging and statistical analysis were done with Openlab and Excel (Microsoft, Seattle, WA) and curve fitting with Origin (Origin Lab, Northampton, MA). The time-lapse image stacks were first registered to correct for retinal movements, then a region of interest was drawn around a dye-loaded ganglion or amacrine cell in the ganglion cell layer, and the cell's fluorescence was measured at each time point. Background due to dark current, ambient light, and autofluorescence was estimated in control experiments with unloaded retinas and subtracted from the cell's fluorescence. For single wavelength indicators MEQ and Calcium Green-1, decline of baseline due to dye bleaching and leakage was fitted with a linear decay curve and subtracted from the cell's fluorescence (Fig. 1*A*). The index $\Delta F/F$, where F is the fluorescent intensity obtained at baseline (after baseline correction and background subtraction) and ΔF is the deviation from F at a given time, was used as a measure of change in ionic concentration. Note that because MEQ fluorescence is quenched collisionally by Cl^-, $\Delta F/F$ goes down proportionally with an increase in Cl^- (see APPENDIX). For calcium imaging with the ratiometric indicator fura-2, we computed the ratio of the cell's average fluorescence at 340 to that at 380 nm (F340/F380).

Measuring intracellular chloride with a reference method

To measure intracellular chloride, we compared a cell's unperturbed MEQ fluorescence to its fluorescence when its intracellular chloride was set to a reference value. Internal chloride concentration was equilibrated by adding the K^+/H^+ exchanger nigericin (7 μM) and the Cl^-/OH^- exchanger tributyltin (10 μM) in the presence of high K^+ (Table 1). The Cl^-/OH^- exchanger equilibrates Cl^- across the membrane, and the K^+/H^+ exchanger in presence of high K^+ is used to clamp pH while Cl^- changes (Krapf et al. 1988). As intracellular chloride equilibrated, if intracellular chloride concentration was reduced (i.e., initial intracellular chloride concentration was higher than reference), the baseline-corrected fluorescence increased. Conversely, if intracellular chloride increased, MEQ fluorescence decreased. Thus we first measured the cell's fluorescence in Ames or Ringer, then equilibrated with a single chloride solution and noted the direction and magnitude of fluorescent change. Noise level in constant chloride was estimated by measuring fluorescence over 15 min. Traces were baseline- corrected and normalized, and the fluorescence fluctuations were measured after additional 7 min. This gave a noise level of 2.5% of initial fluorescence; thus only changes >2.5% were considered significant (Fig. 1*B*).

The native intracellular chloride concentration in Ames or Ringer's solutions was calculated as

$$[Cl]_i = [Cl]_{ref} + \frac{\Delta F_{ref}}{F}(K_{50} + [Cl]_{ref})$$

where F is the fluorescence in Ames or Ringer, ΔF_{ref} is the difference between equilibrated fluorescence and the initial fluorescence, K_{50} is

the half quenching constant obtained from the Stern-Volmer plot as described in the following text, and $[Cl^-]_{ref}$ is the equilibrated chloride concentration (see APPENDIX).

We noted that following the switch of solution and before approaching the new steady state value, fluorescence transiently dropped (see Fig. 7*A*). Fukuda et al. (1998) had described a similar phenomenon and attributed it to the optical interference of nigericin and tributyltin. We found that nigericin and tributyltin did not absorb in the spectrum of MEQ excitation and emission and that the initial drop remained after omitting these ionophores. A similar drop was also obtained with a high K^+ solution with normal chloride or with Ames medium containing glutamate, suggesting it is a secondary effect of the depolarization. Similar excitation-induced chloride influx has also been reported by Inglefield and Schwartz-Bloom (1998). We concluded that the initial drop reflects a transient chloride influx due to the high K^+ solution; afterward the ionophores integrate into the membrane and the new steady-state fluorescence reflects the equilibrated chloride level.

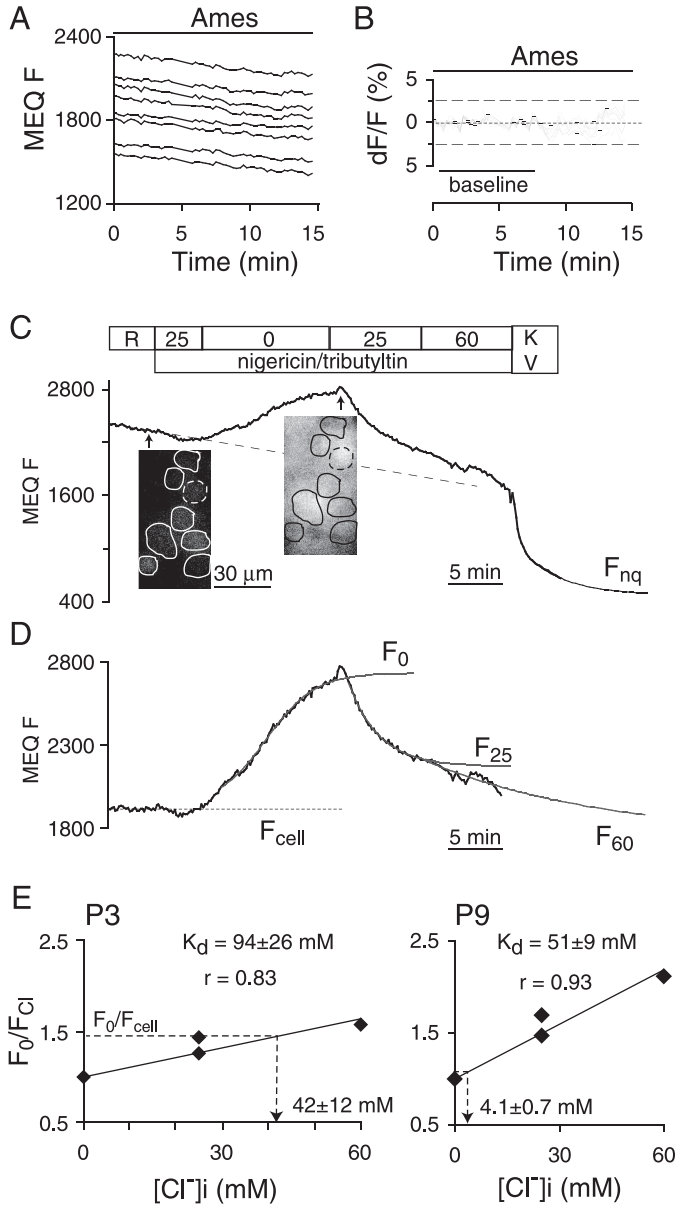

Estimating K_{50} by in vivo MEQ calibration

We first measured a cell's unperturbed MEQ fluorescence, then calibrated MEQ fluorescence by introducing a series of internal chloride concentrations of known values (Table 1). At the end of this series, MEQ fluorescence was completely quenched by adding 150 μM potassium thiocyanate (KSCN) and the K^+ ionophore valinomycin (5 μM); the remaining fluorescence was the un-quenchable component F_{nq}. A cell's fluorescence was corrected for declining baseline as described in the preceding text and corrected for quenching by subtracting F_{nq} (Fig. 1, *C* and *D*). Each solution exchange caused an exponential decrease or increase in fluorescence. The decreases were best fitted with the equation

$$F_t = F_{Cl} + (F_{t=0} - F_{Cl})e^{-t/\tau}$$

and the increases with

$$F_t = \frac{(F_{Cl_{high}} - F_{Cl_{low}})}{1 + e^{(t-t_{1/2})/\tau}} + F_{Cl_{low}}$$

where $F_{Cl_{high}}$ is the initial fluorescent, $F_{Cl_{low}}$ is the steady-state fluorescent after solution change, and $t_{1/2}$ is the time at which the fluorescence reached the middle value between $F_{Cl_{high}}$ and $F_{Cl_{low}}$. We then used the asymptotes of these equations to extrapolate the steady state fluorescence in each solution (F_{Cl}). By calculating the ratio of F at 0 chloride (F_0) over F_{Cl} for each cell, we constructed a Stern-Volmer plot and fit a straight line. The half quenching constant K_{50} was taken as the reciprocal of the line's slope (Marandi et al. 2002; Verkman 1990) (Fig. 1*E*). Although intracellular chloride can be estimated from these plots, this method was not used for many retinas because the procedure was long with low success rate.

Perforated-patch recording

A retina was mounted in a recording chamber and superfused with either bicarbonate-based or bicarbonate-free Ames medium. Before experiments started, the retina was maintained at room temperature.

FIG. 1. Correction and calibration of 6-methoxy-*N*-ethylquinolinium iodide (MEQ) fluorescence. *A*: baseline MEQ fluorescence from 8 cells during continuous perfusion with Ames medium. The decline can be fitted with a linear decay. *B*: setting a criterion level for fluorescence change. Each trace was baseline corrected according to a linear fit for the 1st 7 min, and the difference between the fluorescence and the mean was plotted vs. time. The deviation from 0 in the next 7 min indicates the degree of variability due to imperfect correction; this was <2.5%. Consequently, only changes in fluorescence that exceeded these fluctuations qualified as a response. *C*: uncorrected MEQ fluorescence during nigericin- and tributyltin-induced equilibration with solutions of known chloride concentration (P3; cell with dashed outline). Dashed line shows estimated baseline decay. MEQ fluorescence due to native intracellular chloride concentration was first recorded in Ringer solution (R) and then during equilibration with a series of chloride molarities (as indicated above the trace). At the end of the experiment, a solution of 150 mM KSCN and valionomycin quenched MEQ fluorescence (KV). Quenching was fitted with an exponential curve (gray line), which was extrapolated to nonquenchable fluorescence (F_{nq}). *Inset*: fluorescent images of cells in Ringer solution and 0 mM chloride at times indicated by arrows. *D*: MEQ fluorescence corrected for baseline decay and for nonquenchable fluorescence. During equilibration with 0 mM chloride, fluorescence rose exponentially toward a plateau (F_0); during equilibration with 25 and 60 mM chloride, fluorescence declined toward plateaus (F_{25} and F_{60}). Fitting for the 1st 25 mM chloride is not shown for clarity. Notice that the native fluorescence of the cell (F_{cell}) was lower than F_{25}. *E*: Stern-Volmer plots for cells from P3 (*left*) and P9 (*right*) retinas. Fluorescence was measured from corrected traces. The ratio of MEQ fluorescence at 0 mM chloride (F_0) over MEQ fluorescence at a given chloride level (F_{Cl}) is proportional to the chloride level. The half quenching constant K_{50} is given by the reciprocal of the slope. The native intracellular chloride of the cell can be read out from the plot at F_0/F_{cell} (arrows). Values of K_{50} and $[Cl^-]_i$ are the best estimation ±SE of the estimation; *r*, correlation coefficient.

TABLE 1. *Solutions used for imaging experiments*

	mM							μM	
	Na^+	K^+	Ca^{2+}	Mg^{2+}	Cl^-	Gluconate$^-$	SCN^-	Nigericin/tributyltin	Valinomycin
Ames medium	120	3.6	1.15	1.24	125.3				
Ringers solution	128	5	2	1	139				
0 Ca^{2+} solution	120	3.6		2.39	125.3	139			
0 Cl^- solution		133	2	1	0	139		7/10	
X Cl^- solution		133	2	1	X	139 − X		7/10	
KSCN		150					150		5
X K^+ solution	133 − X	X	2	1	139				

All solutions contained 10–15 mM glucose to adjust osmolality to 296–298 mmol/kg and additional 22.6 mM $NaHCO_3$ or 20 mM HEPES to buffer pH at 7.4.

Cells in the retinal ganglion cell layer were visualized with DIC-infrared optics. Glass electrodes (tip resistance of 2–5 MΩ) were front-filled with gramicidin-free pipette solution (150 mM KCl, 10 mM HEPES, pH 7.25) and backfilled with the pipette solution containing gramicidin D (100–200 μg/ml). Membrane potential was amplified (Axopatch 200B, Axon Instruments, Foster City, CA), sampled at 5 kHz, and stored on a computer (PClamp8 software, Axon Instruments). Data were analyzed with Clampfit (Axon Instruments) and Excel. Gramicidin integrated into the intrapipette membrane 20–60 min after establishing a gigaohm seal, and access resistance stabilized shortly thereafter at values between 60 and 500 MΩ. In general, access resistance was higher for cells in the first postnatal week than those in the second postnatal week (average: 268 vs. 182 MΩ), possibly due to different membrane properties and its ability to incorporate gramicidin. However, E_{GABA} measured with high access resistance did not differ from those with low access resistance, so all the data with a stable access resistance were included. Access resistance dropped to 20–70 MΩ when the patch was ruptured by negative pressure to form the whole cell configuration. This was conducted in each recording to ensure that no occult break-ins occurred, and the perforated-patch recording mode was maintained in all experiments.

During recording, a retina was incubated in a recycled Ames medium containing *O*-(CNB-caged) GABA (1 mM; Molecular Probes), the Na^+ channel blocker tetrodotoxin (TTX, 300 nM), the AMPA receptor antagonist 6-cyano-7-nitroquinoxaline-2,3-dione (CNQX, 10 μM), and the *N*-methyl-D-aspartate (NMDA)-receptor antagonist, 2-amino-7-phosphonoheptanoic acid (AP-7, 100 μM). For retinas before P6, the nicotinic receptor antagonist curare (50 μM) was also added. GABA was focally uncaged at the soma by an ultraviolet laser pulse (5- or 10-ms laser pulse, the uncaging radius was 5 μm in the focal plane) every 20 s (Enterprise II, Coherent Scientific, South Australia, Australia). The apparent reversal potential was corrected for access resistance according to $E_{GABA} = E_{rev} - I_{rev} * R_a$. Using Clampex 8.1 junction potential calculator, we estimated the liquid junction potential in bicarbonate-free medium to be +3.5 mV and that in bicarbonate-based medium to be +3.2 mV. Because these numbers are small and would not affect the difference of E_{Cl} between different developmental stages, the reported reversal potentials were not corrected. If not otherwise noted, all drugs were obtained from Sigma/Aldrich/RBI (St. Louis, MO).

RESULTS

GABAergic neurons stratify in the IPL already at P4

We first determined the time course of developing GABAergic neurons in the mouse retina (Fig. 2). At P2, immunostaining for GABA was positive throughout the retinal layers, but certain cell somas, located near the inner plexiform layer, were more strongly stained. The staining in the inner plexiform layer was evenly distributed and significantly stronger than staining resulting from the secondary antibody itself (3 retina). At P4, most of the somas in the neuroblast layer were light, but some, located at the position of newly migrated horizontal cells, were weakly stained, and the amacrine cells were strongly stained. The inner plexiform layer was now stained more strongly in two distinct strata. P8 resembled P4 except for more frequent amacrine cells and more prominent staining of displaced amacrine cells. At P21, the staining resembled the adult pattern: the inner plexiform layer was now prominently stained in two thin strata and a wider one near the ganglion cell layer. The number of stained amacrine cells in the inner nuclear and ganglion cell layers was fewer than at P8, and horizontal cells were undetectable. Counting cell profiles at P8 and P21, we estimated a reduction of about 30% in the number of cells in the inner nuclear layer and 40% in the ganglion cell layer [2 retinas for each age; total cells counted at P8, $N_{(INL)} = 274$; $N_{(GCL)} = 99$].

GABA switches from excitatory to inhibitory around P6

To determine the time course of the GABA switch, we used fura-2 and recorded calcium responses from neurons located at the ganglion cell layer at different developmental stages. At P0-5, GABA increased calcium in over 99% of the cells (799 cells, 19 retinas; Fig. 3, *A* and *C*). The $GABA_A$ receptor agonist muscimol also increased calcium, and the response was indistinguishable from that evoked by GABA (154 cells, 6 retinas). The GABA or muscimol-evoked calcium increase was robustly and reversibly blocked by the $GABA_A$ receptor antagonist picrotoxin (by 92.5 ± 1.2%; 57 cells, 2 retinas). This confirmed that in the first postnatal week of the mouse retina, GABA is excitatory, and the effect is mediated by ionotropic GABA receptors. The effect of GABA started to change at P6. Then GABA increased calcium in three retinas (54 cells) but failed to do so in two retinas (28 cells), and in one retina, it elicited both responses (33 cells). From P7 to P11, GABA or muscimol consistently failed to increase calcium in over 99% of the cells tested (125 cells, 6 retinas; Fig. 3, *B* and *C*). This indicated that at P6 GABA's excitatory action had started to diminish and that the switch to inhibition was complete by P7.

To test the contribution of endogenous GABA to spontaneous activity, we blocked $GABA_A$ receptor with picrotoxin. At P0–P5, picrotoxin modulated both the amplitude and frequency of calcium transients, but the effect on different cells varied in magnitude and polarity (6 retinas). At P6–P9, picrotoxin increased the frequency of spontaneous calcium transients (11 retinas). At P10–P11, when spontaneous calcium

transients are absent, picrotoxin consistently elicited rhythmic calcium transients that were synchronized across cells, much like those commonly observed at P0–P7 (4 retinas; Fig. 3*B*).

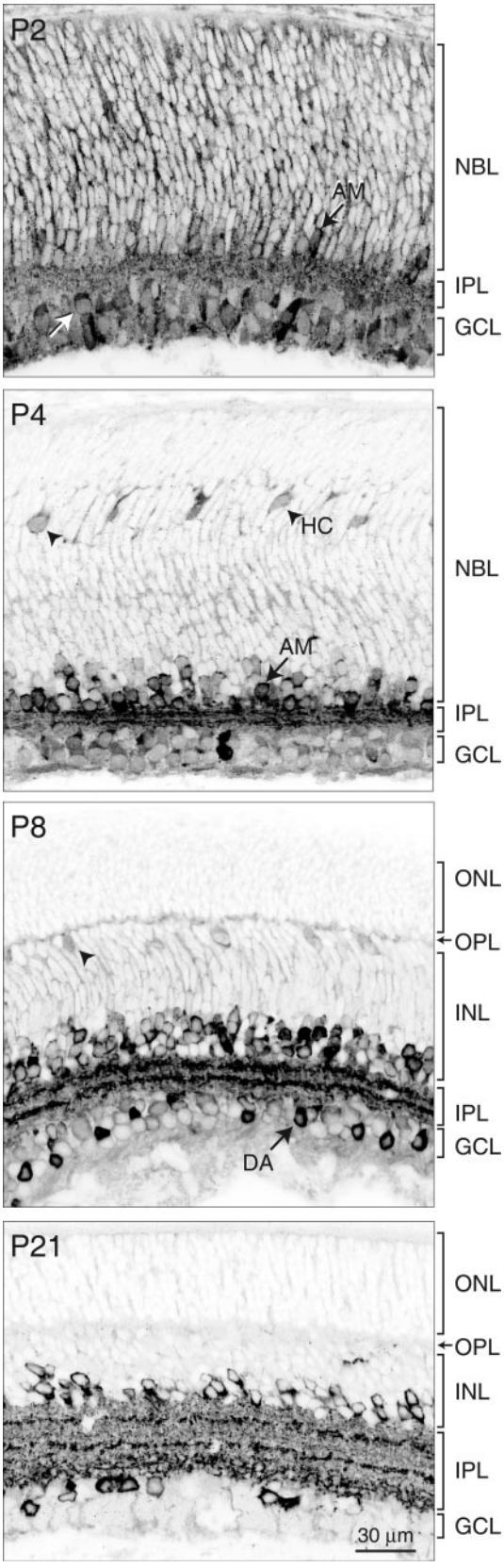

This indicated that by P6 GABA had switched to inhibiting spontaneous activity.

GABA-evoked calcium rise requires extracellular calcium

To determine whether GABA-evoked calcium rise is due to calcium influx through plasma-membrane channels or calcium release from intracellular stores, we initially tried to block calcium channels with cadmium, a general voltage-gated calcium channel blocker. However, cadmium introduced a large artifact: it elevated the ratio of fura-2 fluorescence at 340 and 380 nm, consistent with its high binding affinity to fura-2 (Hinkle et al. 1992). Instead we tested the effect of zero extracellular calcium. After observing GABA's response under normal Ames medium, the retina was switched to zero-calcium solution for 3–4 min; then GABA was applied in the presence of zero-calcium; finally, the retina was switched to normal Ames medium and tested again for response to GABA. On switching to zero-calcium buffer, the intracellular calcium concentration slightly decreased, probably due to a resting calcium conductance. Because of the tendency of GABA-evoked calcium rise to desensitize, only those cells with significant response to GABA in washout were used for analysis. In all such cells (68 cells, 6 retinas), zero-calcium solution greatly diminished GABA-evoked calcium rise (Fig. 4*A*). Thus an influx of calcium through the plasma membrane is the main contributor to GABA-evoked calcium rise in early retina.

GABA-evoked calcium rise persists in a CO_2/HCO_3^--free medium

To test whether the GABA-evoked calcium rise requires an efflux of HCO_3^-, we tested the effect of CO_2/HCO_3^--free (HEPES-based) medium. At P3, GABA consistently evoked calcium rise in over 99% of cells in the absence of HCO_3^-, comparable to that of control (Fig. 4*B*, 165 cells, 7 retinas). Thus the early excitatory action of GABA does not require HCO_3^-, suggesting that the depolarization by GABA is not due to a high permeability to this ion.

GABA switches from decreasing to increasing intracellular chloride around P6

Because the ionotropic GABA receptor conducts mainly chloride current, we next examined the effect of GABA directly on the intracellular chloride level with the chloride indicator MEQ (Fig. 5). At P0–P5, GABA or muscimol increased MEQ fluorescence in over 90% of the cells (230 cells, 9 retinas), indicating a decrease in intracellular chloride. At P6–P12, GABA or muscimol either decreased or caused no significant change in MEQ fluorescence (175 cells, 7 retinas).

To determine if the effects of GABA on chloride and calcium occur at the same cell, some retinas were loaded with both MEQ and the calcium indicator Calcium Green-1 (Fig. 5*A*). At P0–P5, GABA-evoked chloride accumulation was

FIG. 2. GABAergic neurons stratify in the mouse inner plexiform layer by P4. Light micrographs showing GABA immunostaining at P2–P21. →, putative amacrine cells (AM) or displaced amacrine cells (DA); ▲, putative horizontal cells (HC). Note staining in IPL is diffuse at P2 and stratified at P4. NBL, neuroblast layer; IPL, inner plexiform layer; GCL, ganglion cell layer; OPL, outer plexiform layer; INL, inner nuclear layer; ONL, outer nuclear layer; DA, displaced amacrine cells.

accompanied with a calcium increase (112 cells, 4 retinas). At P6–P12, the chloride changes were accompanied with a weak decrease or no change in calcium (84 cells, 3 retinas). At P12, blocking GABA with picrotoxin caused intracellular chloride to deplete steadily and calcium to first recover from the GABA-evoked decrease and then to elevate rapidly before reaching a plateau. The close correlation of chloride and calcium responses suggested that a reversal in the direction of chloride current caused GABA's switch from excitatory to inhibitory, and it further suggested that E_{Cl} changed during development from above to below E_{rest}.

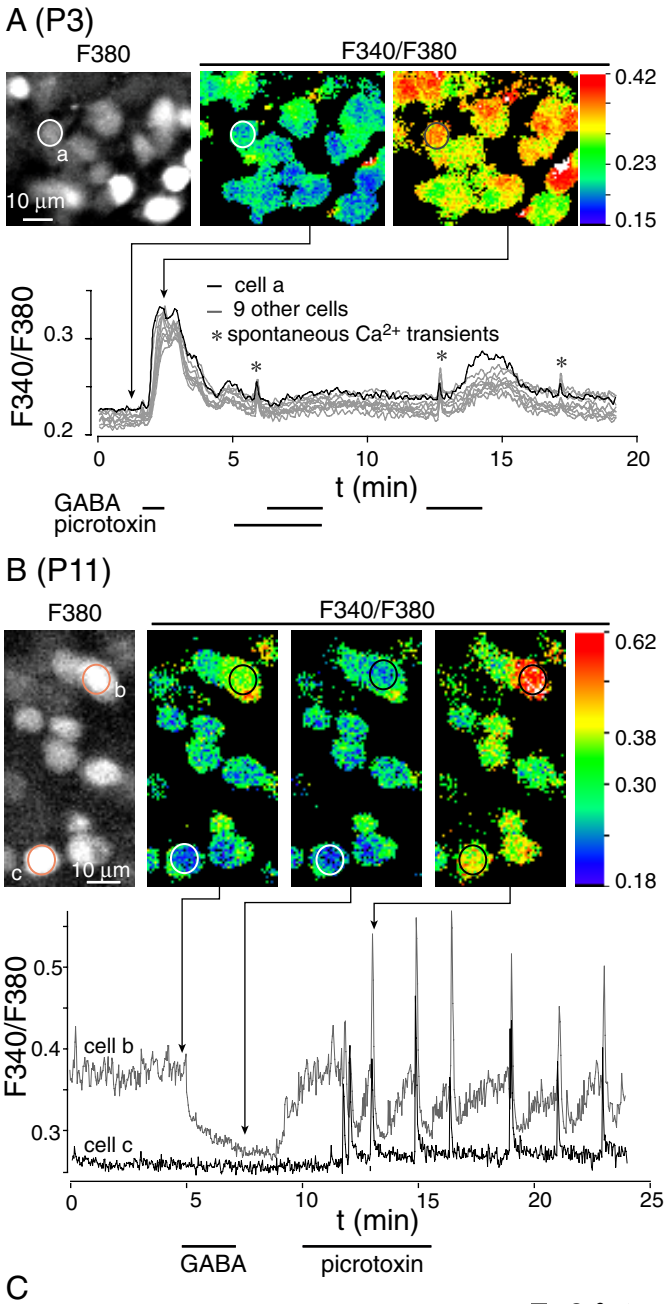

FIG. 3. GABA switches from excitatory to inhibitory around P6. Gray images show fluorescence of cells in the ganglion cell layer at 380 nm excitation. Color images show ratio of fluorescence at 340 and 380 nm excitations (F340/F380 ratio). Traces show time course of F340/F380 ratio. *Top*: at P3, GABA (50 μM) increased calcium in all cells (10 cells are shown, *cell a* is circled in images and represented by a black trace). Response to GABA was largely blocked by coapplication of the $GABA_A$ and $GABA_C$ antagonist (50 μM picrotoxin), and recovered after wash out. *Middle*: at P11, GABA has little effect on calcium in most cells (such as *cell c*). In a few cells (such as *cell b*), GABA decreased calcium; these typically had higher calcium levels than normal. Picrotoxin initiated synchronous spontaneous calcium transients. These transients persisted after picrotoxin was washed out. *Bottom*: developmental profile of calcium responses to GABA and muscimol. Percentage of cells for each response category was calculated for each retina and then averaged over retinas. *R,* number of retinas; *C,* number of cells.

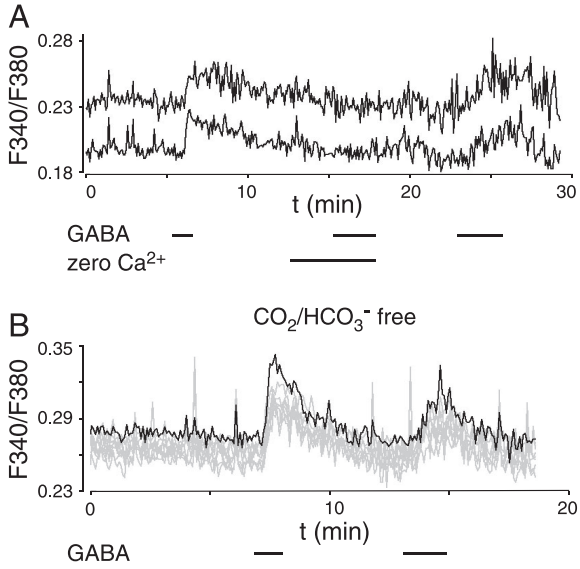

FIG. 4. Ionic dependence of GABA-evoked calcium rise in early reitna. *A*: at P2, Response to GABA (120 μM) was largely blocked by 0-calcium solution, and recovered after returning to normal Ames medium. Two traces from different cells of the same experiment are shown. *B*: at P3, GABA (50 μM) repeatedly evoked calcium rise in bicarbonate-free solution. Traces from 8 cells are shown; 1 is highlighted in black.

E_{Cl} measured with gramicidin-perforated-patch recording

To test whether E_{Cl} indeed changes during development, we used the gramicidin-perforated-patch mode of recording on neurons in the ganglion cell layer. A cell was voltage clamped, its membrane potential was systematically varied using either a step or a ramp protocol, GABA was uncaged focally near the soma, and the reversal potential of the GABA response, E_{GABA}, was calculated (Fig. 6, *A* and *B*). To test whether HCO_3^- contributes to E_{GABA}, in some experiments, HCO_3^- was removed and replaced with HEPES. E_{GABA} measured in either buffer was indistinguishable, suggesting HCO_3^- does not contribute significantly to E_{GABA} in agreement with the calcium imaging results. Pooling data from all experiments, the average E_{GABA} at P1–P3 was -45 ± 3 mV (7 cells), whereas

at P7–P11, it was significantly lower with a mean value of −60 ± 2 mV (10 cells; $P < 0.001$, *t*-test; Fig. 6, *C* and *D*). After a perforated-patch recording, we disrupted the membrane using negative pressure, instituting the whole cell recording mode. This brought E_{GABA} close to the chloride Nernst potential (5 mV) calculated using the composition of the intrapipette and extracellular media. This ensured that the perforated-patch recording mode was maintained throughout the recording period, and no occult breaking occurred. From our perforated-patch data, assuming that the predominant permeant ion for GABA responses is chloride, we calculate (using the Nernst equation) that the intracellular chloride concentration was 22 ± 2 mM for P1–P3 and 12 ± 1 mM for P7–P11.

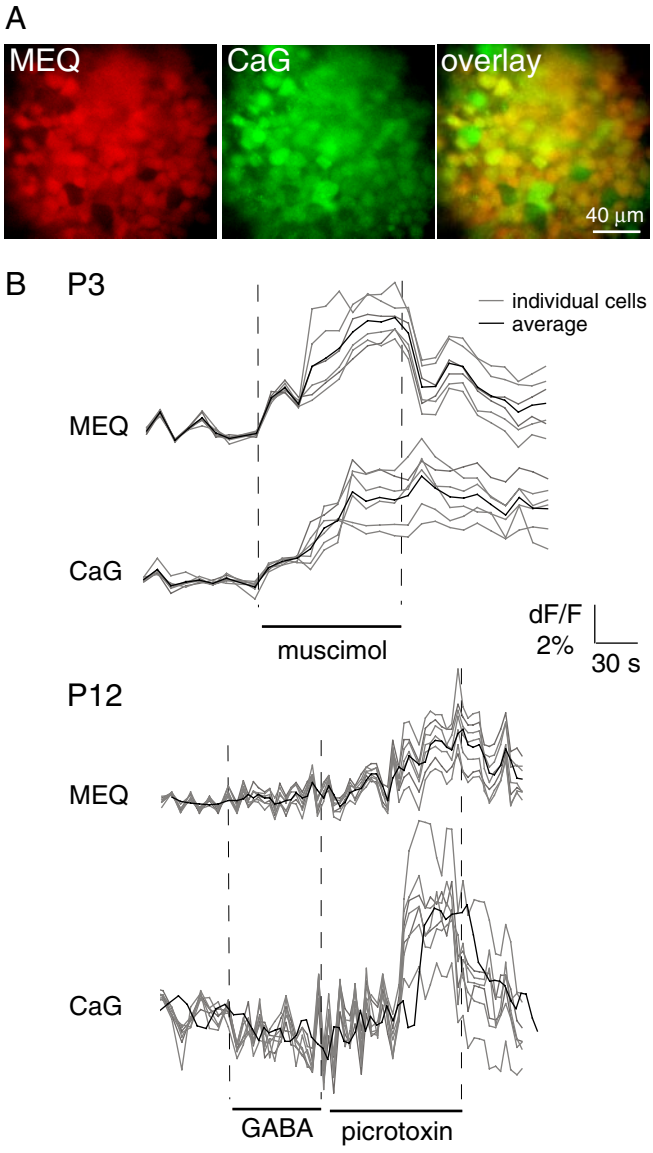

FIG. 5. GABA switches from increasing to decreasing chloride around P6. *Top*: whole-mount mouse retina (P5) loaded with the chloride indicator MEQ (*left*) and the calcium indicator Calcium Green-1 (CaG); most of the cells in the ganglion cell layer were successfully loaded with both dyes (overlay).*Middle*: simultaneous measurements of MEQ and CaG fluorescence ($\Delta F/F$). An increase in MEQ fluorescence indicates a decrease in chloride whereas an increase in CaG fluorescence indicates an increase in calcium. Gray traces, measurements from individual neurons; black trace, the average of all cells shown. Dashed vertical lines mark the time of solution change. At P3, muscimol reduced chloride and increased calcium (sampling rate 0.1 Hz, 6 cells). At P12, GABA produced no significant change in chloride and slightly decreased calcium. Picrotoxin reduced chloride and increased calcium to the level before GABA; it then further increased calcium to a new plateau (sampling rate 0.25 Hz, 2-point moving average, 7 cells). *Bottom*: Summary of developmental changes of chloride response to GABA and muscimol. *R*, number of retinas; *C*, number of cells.

Intracellular chloride level measured by chloride reference

To directly measure the intracellular chloride, we compared intracellular chloride to a set of specific reference chloride solutions. Reference chloride concentrations in these experiments were chosen according to intracellular chloride levels that would set E_{Cl} to values critically affecting chloride flux and its downstream effect on calcium flux or spiking (Table 2). There were three possible responses: if the initial intracellular chloride concentration was lower than the reference, fluorescence would be quenched by chloride influx; if intracellular chloride was higher than reference, fluorescence would increase with chloride efflux; if intracellular chloride was equal to reference, there would be no significant change (Fig. 7*A*). For each reference concentration, we counted the number of cells giving a certain response (Fig. 7*B*, Table 3). In general, all neighboring cells responded in a similar manner, suggesting amacrine and ganglion cells have similar chloride concentrations.

We plotted developmental profile of chloride concentration relative to reference concentrations of 22 and 30 mM. Chloride concentration above these values would bring E_{Cl} to the thresholds for low- and high-voltage-activated calcium channels, respectively. At P0–P5, when GABA universally evoked a calcium rise, >75% of cells had intracellular chloride >22 mM, potentially allowing GABA to activate low-voltage calcium channels (Fig. 8*A*). More than 50% of cells had intracellular chloride >30 mM, potentially allowing GABA to activate high-voltage calcium channels. At P6, the time of GABA's switch, the percentage of cells with over 30 mM chloride dropped sharply to 22%. By P8, when GABA completed its switch, rarely any cell had >30 mM chloride, yet about half of the cells still had >22 mM. At P10–P11, intracellular chloride in all cell further dropped <22 mM.

To obtain specific values of intracellular chloride level from the reference experiments, we modified the Stern-Volmer equation to describe the relationship between two chloride concentrations and the difference between their steady-state fluorescence ΔF_{ref} (*Eq. 1* in METHODS; see APPENDIX). We first estimated the average K_{50} value for retina from in vivo MEQ calibration experiments. For two retinas (P3 and P9), we obtained an average K_{50} of 75 mM (17 cells; see Fig. 1). We then measured the median $\Delta F_{ref}/F$ from each chloride refer-

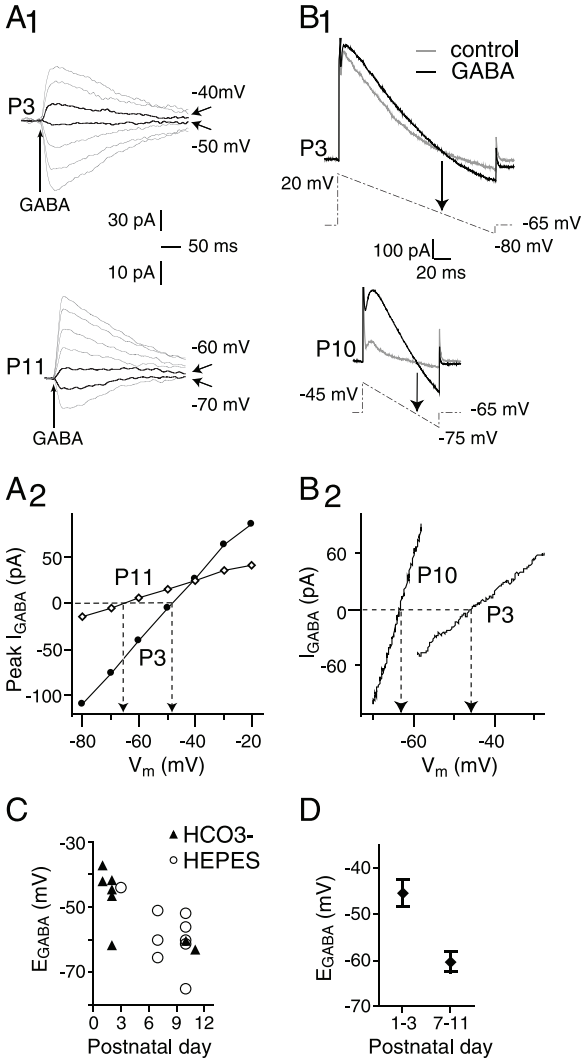

FIG. 6. E_{GABA} declines during development. GABA-evoked currents were recorded from neurons in ganglion cell layer using gramicidin-perforated-patch recordings. *A*: determination of E_{GABA} using voltage steps followed by GABA application (*cell* of P3 was buffered with HEPES, *cell* of P11 with HCO_3^-). *A1*: a cell was stepped from a holding voltage of −65 mV to a command voltage of −80 to +20 mV in 10-mV increments. The command voltage was held for 7 s to allow voltage-dependent currents to inactivate, then GABA was focally uncaged near the soma (5-ms laser pulse, 1-mM caged GABA), and the command voltage was held for a further 3 s. Traces show GABA-evoked currents; dark traces show currents for voltage commands near the reversal potential. *A2*: current-voltage plots are from peak currents of the cells above. After correction for access resistance, E_{GABA} was −45 mV at P3 and −59 mV at P11. *B*: determination of E_{GABA} with voltage ramps during GABA application (HEPES-based Ames medium). *B1*: superimposed current responses to voltage ramps with (black trace) and without (gray trace) GABA from cells at P3 and P10. The voltage range of each ramp was adjusted to flank the expected reversal potential of GABA and is indicated for each cell under the current trace. Initial capacitance current was clipped. *B2*: current-voltage plots are obtained by subtracting the control trace from the GABA trace. After access resistance correction, E_{GABA} was −40 mV at P3 and −61 mV for the P10 cell. *C*: E_{GABA} at different postnatal ages from both methods. Each data point is from 1 cell. Data from HCO_3^--based buffer (triangles) and HEPES-based buffer (circles) are similar. *D*: values of E_{GABA} were pooled into early (P1–P3; $n = 7$) and late (P7–P11; $n = 10$) stages. Data are means ± SE.

ence experiment (Fig. 7*A*). Experiments with different reference solutions gave similar results, and were pooled. At P0–P5, the average intracellular chloride concentration was 29 mM with a range of 20–40 mM, at P6, it started to decline, averaging at 18 mM with a range of 10–30 mM, and after P6, it further declined to 14 mM with a range of 5–20 mM (Fig. 8*B*).

DISCUSSION

We report here that GABA application elicits an increase in intracellular calcium until P6, and thereafter it either has no effect on intracellular calcium or reduces it. Between P6 and P11, blocking GABA receptors enhances or elicits spontaneous calcium activity, suggesting that GABA responses are inhibitory at this developmental stage. The switch starts at P6 and is complete by P7. Correlated with this time line, GABA evokes an efflux of chloride before P6 and an influx afterward. During this shift, E_{GABA} declines by ~15 mV (from about −45 to −60 mV), and intracellular chloride level declines from 29 to 14 mM.

Pros and cons of intracellular chloride measurement methods

Measurements of chloride are prone to various types of error. To address this, we used several methods and found reasonable agreement. Gramicidin-perforated patch measures GABA reversal potentials under conditions of unperturbed intracellular chloride. From these data, intracellular chloride can be calculated based on the assumption that $E_{GABA} = E_{Cl}$. This is true only if the GABA receptor is relatively impermeant to bicarbonate ions. The accuracy of the measurement also relies on a good space clamp, which might be difficult to obtain, especially early in development when cells are highly coupled (Becker et al. 2002; Penn et al. 1994). In our experiment, we tested E_{GABA} both in the presence and absence of $HCO3^-$ and alleviated the space-clamp problem by uncaging GABA focally onto the soma, so that much of the GABA-evoked current was close to the electrode.

TABLE 2. *Choice of reference chloride concentration*

Critical Membrane Potentials	References	$E_{critical}$, mV	$[Cl^-]_i$ when $E_{Cl} = E_{critical}$, mM
E_{rest} (low end of range)	1, 2	−67	10
E_{rest} (high end of range)	1, 3	−56	15
LVA I_{Ca} activation, low end of spike threshold	1, 4, 5	−46	22
LVA, HVA I_{Ca} activation	4	−38	30
HVA I_{Ca} activation, High end of spike threshold	1, 4	−30	40

For GABA to depolarize, the membrane to reach a certain threshold (first 3 columns), E_{Cl} must be equal to or more positive than that threshold. Using the Nernst equation, we calculated the intracellular chloride concentration $[Cl^-]_i$ that will establish E_{Cl} at the level of such thresholds (4th column). The calculated $[Cl^-]_i$ were then chosen as reference in the experiments presented in Table 3. When $E_{cl} = E_{rest}$, no polarization by GABA is expected. Parameters for the Nernst equation were taken from our experimental condition of fura-2 calcium imaging (i.e., extracellular chloride concentration = 125 mM, T = 33°C). LVA I_{Ca}, low-voltage-activated calcium current; HVA I_{Ca}, high-voltage-activated calcium current; spike refers to sodium spike. References: [1]Zhou (1998), [2]Koizumi et al. (2004), [3]Wang et al. (1999), [4]Schmid and Guenther (1996), [5]Guenther et al. (1999).

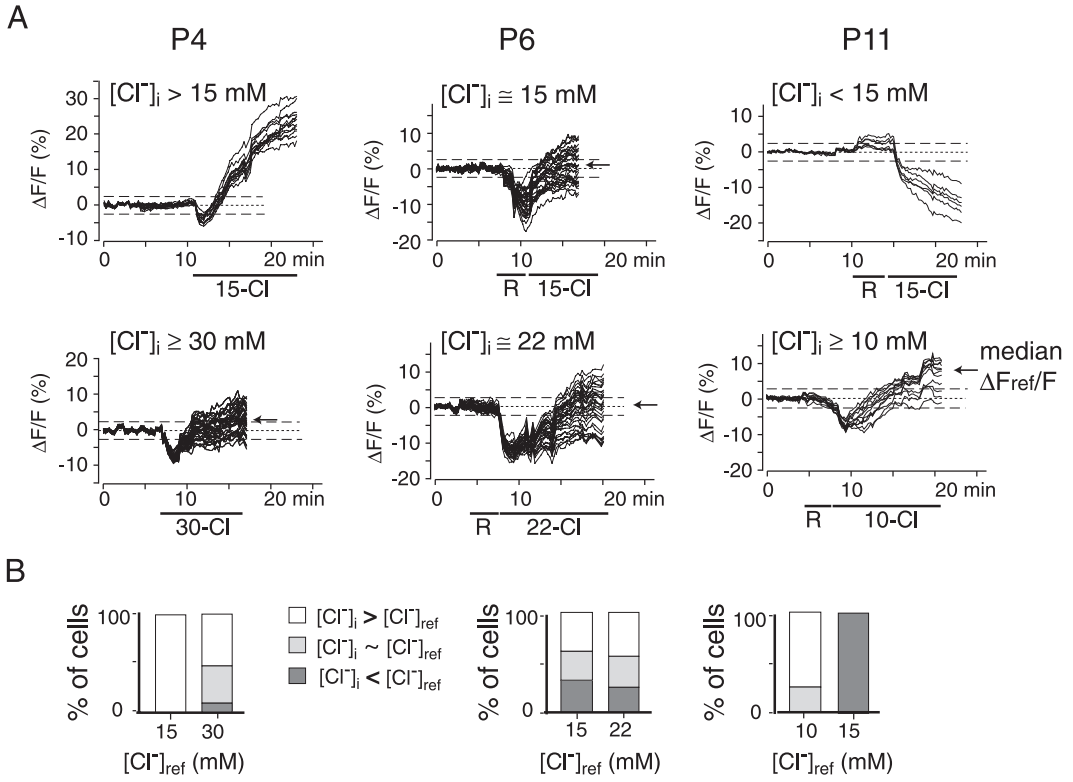

FIG. 7. Determination of intracellular chloride concentration by chloride reference. *A*: comparison of the intracellular chloride to a reference level. After recording the baseline of MEQ fluorescence in Ames medium with undisturbed chloride, intracellular chloride was clamped to a reference chloride. After an initial drop (see METHODS), the fluorescence reached a new steady-state level, which was either higher than the reference (indicating initial chloride was higher) or lower (indicating initial chloride was lower). A change within 2.5% above and below (dashed lines) the baseline (dotted line) was considered near the reference. Representative experiments at 2 references are shown for each postnatal day. R, Ringer solution; $\Delta F_{ref}/F$, steady-state fluorescence change from baseline under a given chloride reference. ←, the median $\Delta F_{ref}/F$ for each trial. *B*: stacked column histogram of chloride in 3 categories (above, near, or below the reference) for the experiments shown in *A*. At P4, chloride in all cells was higher than 15 mM (in 1 retina) and near or above 30 mM (in another retina). At P6, chloride levels distributed around 15 and 22 mM. At P11, chloride in all cells was lower than 15 mM (in 1 retina) and near or above 10 mM (in another retina).

The chloride-sensitive fluorescent dyes provide direct measurements of intracellular chloride and permit assessment of its spatial distribution. MEQ and its relatives MQAE and SPQ have been used to report relative chloride change and absolute chloride concentration in several brain regions (Fukuda et al. 1998; Ikeda et al. 2003; Inglefield and Schwartz-Bloom 1999; Kaneko et al. 2004; Marandi et al. 2002; Thoreson and Bryson 2004; Thoreson et al. 2000). MEQ is especially appealing among its relatives due to its improved cell retention and relatively high sensitivity, as reflected by a K_{50} of 50–100 mM found by this study and in other neurons (between 32 and 87 mM) (Chistina et al. 1999; Fukuda et al. 1998; Ikeda et al. 2003; Inglefield and Schwartz-Bloom 1998). However, chloride concentration measurement based on MEQ calibration carries a large error (~30%) due to change in fluorescence baseline decay after introducing ionophores and high K^+ (Nakamura et al. 1997). In addition, many cells do not survive the toxicity of long incubation in ionophores and high K^+ (see also Kaneko et al. 2001).

To mitigate some of the problems associated with MEQ calibration, we developed the chloride reference method. It substantially shortens the experimental procedure and greatly enhances cell survival. It directly answers the question whether the intracellular chloride level is higher or lower than a certain

TABLE 3. *Developmental changes of intracellular chloride*

	Relative Frequency of $[Cl^-]_i \geq [Cl^-]_{ref}$, %						
$[Cl^-]_{ref}$	P0	P2–P3	P4	P5	P6	P7–P8	P10–P11
10 mM							78 ± 11 (4:74)
15 mM		100 (1:38)	100 (1:13)	100 (1:33)	80 ± 12 (2:54)	100 (1:27)	56 ± 28 (3:39)
22 mM	83 ± 27 (2:74)	100 ± 0 (2:49)	77 ± 5 (2:54)	90 (1:10)	73 ± 10 (3:139)	50 ± 50 (2:42)	0 (1:17)
30 mM	51 ± 49 (2:73)	89 ± 11 (2:63)	64 ± 32 (4:69)	58 ± 9 (6:254)	22 ± 20 (5:163)	4 ± 4 (2:48)	0 ± 0 (2:39)
40 mM	2 ± 2 (2:101)			30 ± 30 (2:82)		0 (1:26)	
Total retinas	6	5	7	10	10	6	10

Numbers in cells are the percentage of neurons at each postnatal age with intracellular chloride ($[Cl^-]_i$) higher than the reference value ($[Cl^-]_{ref}$). Data are the means ± SE of percentage cells averaged from different retinas. Values in parentheses report number of retinas and number of neurons for each age group. More experiments were conducted with $[Cl^-]_{ref}$ close to $[Cl^-]_i$, (indicated by a frequency close to 50%) because this allows more accurate estimation of $[Cl^-]_i$, (for explanation see APPENDIX).

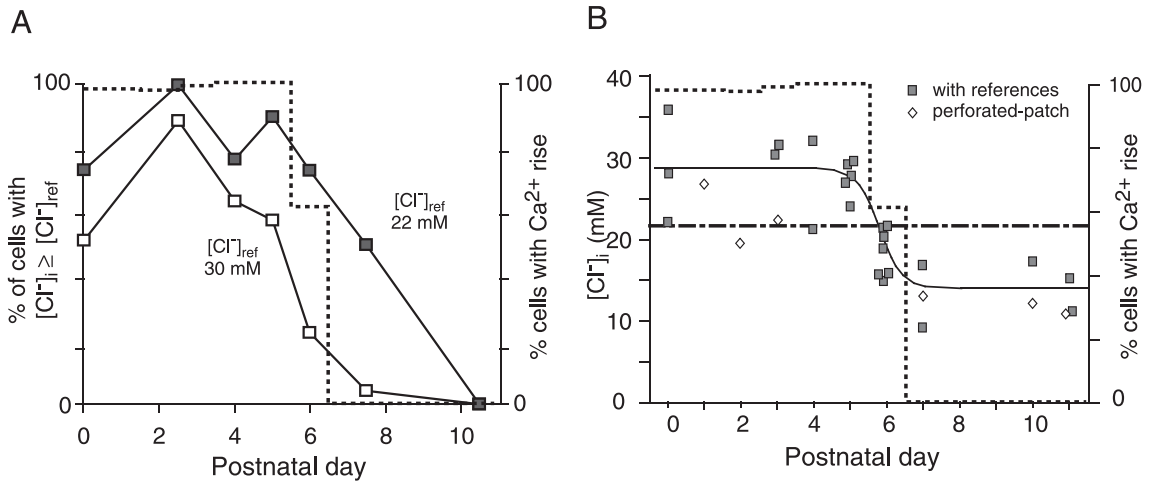

FIG. 8. Intracellular chloride concentration shifts from potentially excitatory to inhibitory range at P6. *A*: percentage cells with intracellular chloride concentration ≥22 mM (■) and 30 mM (□) vs. age. Certain data are binned into a 2-day window (P2–P3, P7–P8. and P10–P11). Dotted line, concomitant change of calcium responses to GABA (from Fig. 3). *B*: intracellular chloride concentrations converted from the medians of $\Delta F_{ref}/F$ (← in Fig. 7*A*) vs. age; only trials in which the flourescence reached a plateau after a solution change were used for these calculations. —, fit of values obtained from the reference experiments using the Boltzmann equation. At P6, intracellular chloride concentration dropped sharply from 29 to 14 mM. Intracellular chloride concentrations measured with gramicidin-perforated patch recordings (◇) are from Fig. 6. Dash-dotted line, intracellular chloride level required for GABA to activate low-voltage-activated calcium channels. Data points above this line indicate potential for calcium rise by GABA. · · · as in *A*.

level, which in our experiment was selected according to predictions made about GABA's function. Finally, if the reference concentration is chosen to be near the intracellular chloride level, the method can improve the accuracy of chloride measurement.

Intracellular chloride in the developing retina

By combining results from the different methods, we find that intracellular chloride can be divided into three stages. During the first postnatal week, intracellular chloride averaged 29 mM corresponding to an E_{Cl} of –39 mV, which is 21 mV more depolarized than average E_{rest} (−60 mV). This is sufficiently depolarized to trigger most voltage-activated calcium and sodium channels (Table 2). Across cells, there was some variation in chloride concentration (20–40 mM). Thus some cells had a predicted E_{Cl} as hyperpolarized as −48 mV, which is below threshold for voltage-activated calcium channels. This might explain why a small percentage of cells failed to show a calcium rise at P1–P2.

During the transition period (P6), intracellular chloride in most cells exceeded 22 mM, which predicts an E_{Cl} above −46 mV, the threshold of low-voltage-activated calcium channels. This suggests that most cells would respond to GABA with a calcium increase, which is indeed what we found by fura-2 calcium imaging. At P7, although the average intracellular chloride was about 14 mM, corresponding to an E_{Cl} of −58 mV, there were still ~50% of cells >22 mM; yet none responded with calcium increase. In rat, expression of major voltage-gated calcium channels shifts from low-voltage-activated calcium channels to high-voltage-activated calcium channels at around P6–P9 (Guenther et al. 1994; Schmid and Guenther 1996). Similar depolarizing shift in threshold for

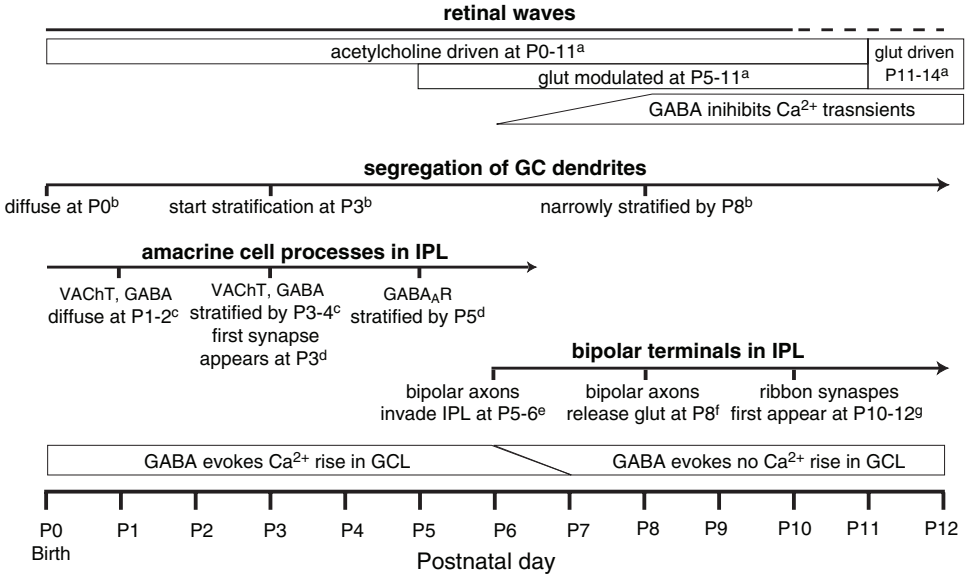

FIG. 9. Summary of temporal sequence of GABA's action in developing mouse retina and timing of major developmental events in the inner plexiform and ganglion cell layers. Where mouse data are not available, rat data are quoted. Glut, glutamate; GC, ganlglion cells; VachT, vesicular acetylcholine transporter; IPL, inner plexiform layer; GCL, ganglion cell layer. Sources of data: [a], Bansal et al. (2000); [b], Diao et al. (2004); [c], Stacy and Wong (2003); [d], Fisher (1979), Sassoè-Pognetto and Wässle (1997) (rat); [e], Ueda et al. (1997); [f], Sherry et al. (2003); [g], Olney (1968), Fisher (1979).

calcium activation have been observed for cultured hippocampal neuron (Ganguly et al. 2001). Thus the shift in calcium activation toward more depolarized potentials might account for the failure of GABA to evoke calcium increase at P7.

Finally, during the second postnatal week, intracellular chloride ranged from 5 to 20 mM, which predicts an E_{Cl} of −85 to −48 mV. This entire range of voltages would allow GABA to hyperpolarize or shunt the cell but would not trigger voltage-activated channels as was indeed demonstrated by calcium imaging during this developmental period. The average chloride concentration (14 mM) predicts an E_{Cl} of −58 mV and the perforated-patch recordings gave an average of −60 mV. These values are between the E_{Cl} measured in adult mudpuppy ganglion cells using a chloride-sensitive electrode (−49 mV) (Miller and Dacheux 1983) and in adult goldfish amacrine cells using gramicidin-perforated patch (−76 mV) (Watanabe et al. 2000). This might suggest that E_{Cl} approaches adult values by the end of the first postnatal week.

Timing and functional implication of GABA's actions

GABA switches from excitatory to inhibitory at P6, the same time as bipolar cells start to invade the inner plexiform layer (Fig. 9). Such coincidence between the time of GABA's switch and the time of bipolar cell axonal arborizations also occurs in ferret, chicken, and rabbit (Catsicas and Mobbs 2001; Fischer et al. 1998; Zhou 2001). It is thus reasonable to suggest that, as in other brain regions (Ben Ari 2002), GABA provides the major excitatory role before glutamate released from bipolar cells takes over.

Excitatory activity is important for a variety of developmental processes, most notably for refinement and stabilization of synaptic connections (Harms et al. 2005; Katz and Shatz 1996; Lichtman and Colman 2000; Wiesel 1982). In retina, we suggest that before the switch, GABA released from amacrine cells could contribute to activity-dependent refinement of synaptic connections from amacrine to ganglion cells. This hypothesis stems from several observations. First, GABAergic amacrine cells stratify before ganglion cells, suggesting they could provide laminar cues (Karne et al. 1997). Furthermore, when ganglion cells start to stratify, GABA is still excitatory (Fig. 9), suggesting the cues could result from local excitation by GABA. Second, excitation is indeed important for normal stratification as shown in later development, when glutamate provides the major excitation. At this stage of development, preventing glutamate release from ON bipolar terminals disrupts the segregation of ganglion cell dendrites into ON and OFF sublamina (Bodnarenko and Chalupa 1993; Bodnarenko et al. 1995). Third, early in development, the major excitation is provided by acetylcholine and GABA. Cholinergic amacrine cells may provide laminar cues for one type of ganglion cells but not for the others (Stacy and Wong 2003), leaving GABA as the main candidate. Fourth, similar role for GABA has been demonstrated in the outer retina, where GABA is required for the normal development of cone to horizontal cells synapses (Huang and Redburn 1996). Our findings suggest that disrupting the accumulation of intracellular chloride could be used to test the contribution of GABA's excitation to the development of the inner retina.

Later, when GABA ceases to evoke calcium rise, blocking ionotropic GABA receptor elicits synchronized calcium transients in all cells. Similar results were found in ferret (Fischer et al. 1998), turtle (Sernagor et al. 2003), and rabbit (Syed et al. 2004), suggesting a common role of GABA in restricting and terminating retinal waves later in development.

APPENDIX

Deriving native intracellular chloride concentration from steady-state fluorescence change obtained by clamping intracellular chloride to a reference solution

Chloride quenches MEQ fluorescence in a concentration-dependent manner according to the Stern-Volmer equation (Verkman 1990)

$$\frac{F_0}{F_{Cl}} = 1 + \frac{[Cl]}{K_{50}} \tag{A1}$$

Where K_{50} is the reciprocal of the Stern-Volmer quenching constant and is equal to the concentration that quenches 50% of the maximum quenchable signal (Marandi et al. 2002); F_0 and F_{Cl} are the baseline-corrected quenchable signals at zero chloride and at a given chloride concentration, respectively.

Rearranging the equation gives

$$F_0 * K_{50} = F_{Cl} * (K_{50} + [Cl]) \tag{A2}$$

Because the left side of the equation is constant for a given MEQ concentration, the right side can be applied to the steady states in initial $[Cl^-]_i$ and $[Cl^-]_{ref}$; this gives

$$F_{Cell} * (K_{50} + [Cl]_i) = F_{ref} * (K_{50} + [Cl]_{ref}) \tag{A3}$$

Where F_{Cell} and F_{ref} are the steady-state fluorescence values in $[Cl^-]_i$ and $[Cl^-]_{ref,}$ respectively.

Rearranging *Eq. A3* gives

$$\frac{K_{50} + [Cl]_i}{K_{50} + [Cl]_{ref}} = \frac{F_{ref}}{F_{Cell}} \tag{A:4}$$

Subtracting 1 from both sides, and introducing $\Delta F_{ref}/F = (F_{ref} - F_{cell})/F_{cell}$ into *Eq. A4* yields

$$\frac{[Cl]_i - [Cl]_{ref}}{K_{50} + [Cl]_{ref}} = \frac{\Delta F_{ref}}{F} \tag{A5}$$

Rearranging gives intracellular chloride concentration as a function of $\Delta F_{ref}/F$

$$[Cl]_i = [Cl]_{ref} + \frac{\Delta F_{ref}}{F}(K_{50} + [Cl]_{ref}) \tag{A6}$$

Note that when $\Delta F_{ref}/F = 0$, $[Cl^-]_i = [Cl^-]_{ref}$; when $\Delta F_{ref}/F$ is small, an error in K_{50} estimation has small consequence on $[Cl^-]_i$ measurement; when $[Cl^-]_{ref} = 0$, *Eq. A6* becomes the Stern-Volmer *Eq. A1*.

ACKNOWLEDGMENTS

We are grateful to P. Sterling and Penn Neuroscience Graduate Group for continuing support, to P. Sterling, R. G. Smith, and M. Feller for reading the manuscript, to M. Fina for excellent technical assistance, and to Drs. Phil G. Haydon and Michael P. Nusbaum for helpful discussions.

GRANTS

This work was supported by National Institutes of Health Grants EY-11105 to N. Vardi, EY-00828 to P. Sterling, EY-13333 to M. A. Freed, and NS-32403 and NS-38572 to D. A. Coulter.

REFERENCES

Bansal A, Singer JH, Hwang BJ, Xu W, Beaudet A, and Feller MB. Mice lacking specific nicotinic acetylcholine receptor subunits exhibit dramatically altered spontaneous activity patterns and reveal a limited role for

retinal waves in forming ON and OFF circuits in the inner retina. *J Neurosci* 20: 7672–7681, 2000.

Becker DL, Bonness V, Catsicas M, and Mobbs P. Changing patterns of ganglion cell coupling and connexin expression during chick retinal development. *J Neurobiol* 52: 280–293, 2002.

Ben Ari Y. Developing networks play a similar melody. *Trends Neurosci* 24: 353–360, 2001.

Ben Ari Y. Excitatory actions of GABA during development: the nature of the nurture. *Nat Rev Neurosci* 3: 728–739, 2002.

Bodnarenko SR and Chalupa LM. Stratification of ON and OFF ganglion cell dendrites depends on glutamate-mediated afferent activity in the developing retina. *Nature* 364: 144–146, 1993.

Bodnarenko SR, Jeyarasasingam G, and Chalupa LM. Development and regulation of dendritic stratification in retinal ganglion cells by glutamate-mediated afferent activity. *J Neurosci* 15: 7037–7045, 1995.

Bormann J, Hamill OP, and Sakmann B. Mechanism of anion permeation through channels gated by glycine and gamma-aminobutryic acid in mouse cultured spinal neurons. *J Physiol* 385: 243–286, 1987.

Catsicas M and Mobbs P. $GABA_B$ receptors regulate chick retinal calcium waves. *J Neurosci* 21: 897–910, 2001.

Chistina GA, Inglefield JR, Schwartz-Bloom RD, Devaud LL, and Morrow AL. Fluorescence imaging of $GABA_A$ receptor-mediated intracellular [Cl^-] in P19-N cells reveals unique pharmacological properties. *Brain Res* 827: 1–11, 1999.

Diao L, Sun W, Deng Q, and He S. Development of the mouse retina: emerging morphological diversity of the ganglion cells. *J Neurobiol* 61: 236–249, 2004.

Ehrlich I, Lohrke S, and Friauf E. Shift from depolarizing to hyperpolarizing glycine action in rat auditory neurons is due to age-dependent Cl^- regulation. *J Physiol 520 Pt* 1: 121–137, 1999.

Eilers J, Plant TD, Marandi N, and Konnerth A. GABA-mediated Ca^{2+} signaling in developing rat cerebellar Purkinje neurones. *J Physiol* 536: 429–437, 2001.

Firth SI, Wang CT, and Feller MB. Retinal waves: mechanisms and function in visual system development. *Cell Calcium* 37: 425–432, 2005.

Fischer KF, Lukasiewicz PD, and Wong RO. Age-dependent and cell class-specific modulation of retinal ganglion cell bursting activity by GABA. *J Neurosci* 18: 3767–3778, 1998.

Fisher LJ. Development of synaptic arrays in the inner plexiform layer of neonatal mouse retina. *J Comp Neurol* 187: 359–372, 1979.

Fukuda A, Tanaka M, Yamada Y, Muramatsu K, Shimano Y, and Nishino H. Simultaneous optical imaging of intracellular Cl^- in neurons in different layers of rat neocortical slices: advantages and limitations. *Neurosci Res* 32: 363–371, 1998.

Ganguly K, Schinder AF, Wong ST, and Poo M. GABA itself promotes the developmental switch of neuronal GABAergic responses from excitation to inhibition. *Cell* 105: 521–532, 2001.

Guenther E, Rothe T, Taschenberger H, and Grantyn R. Separation of calcium currents in retinal ganglion cells from postnatal rat. *Brain Res* 633: 223–235, 1994.

Guenther E, Schmid S, Reiff D, and Zrenner E. Maturation of intrinsic membrane properties in rat retinal ganglion cells. *Vision Res* 39: 2477–2484, 1999.

Harms KJ, Tovar KR, and Craig AM. Synapse-specific regulation of AMPA receptor subunit composition by activity. *J Neurosci* 25: 6379–6388, 2005.

Hinkle PM, Shanshala ED, and Nelson EJ. Measurement of intracellular cadmium with fluorescent dyes. Further evidence for the role of calcium channels in cadmium uptake. *J Biol Chem* 267: 25553–25559, 1992.

Huang BO and Redburn DA. GABA-induced increases in $[Ca^{2+}]_i$ in retinal neurons of postnatal rabbits. *Vis Neurosci* 13: 441–447, 1996.

Ikeda M, Yoshioka T, and Allen CN. Developmental and circadian changes in Ca^{2+} mobilization mediated by $GABA_A$ and NMDA receptors in the suprachiasmatic nucleus. *Eur J Neurosci* 17: 58–70, 2003.

Inglefield JR and Schwartz-Bloom RD. Activation of excitatory amino acid receptors in the rat hippocampal slice increases intracellular Cl^- and cell volume. *J Neurochem* 71: 1396–1404, 1998.

Inglefield JR and Schwartz-Bloom RD. Fluorescence imaging of changes in intracellular chloride in living brain slices. *Methods* 18: 197–203, 1999.

Kaila K, Pasternack M, Saarikoski J, and Voipio J. Influence of GABA-gated bicarbonate conductance on potential, current and intracellular chloride in crayfish muscle fibers. *J Physiol* 416: 161–181, 1989.

Kaneko H, Nakamura T, and Lindemann B. Noninvasive measurement of chloride concentration in rat olfactory receptor cells with use of a fluorescent dye. *Am J Physiol Cell Physiol* 280: C1387–C1393, 2001.

Kaneko H, Putzier I, Frings S, Kaupp UB, and Gensch T. Chloride accumulation in mammalian olfactory sensory neurons. *J Neurosci* 24: 7931–7938, 2004.

Karne A, Oakley DM, Wong GK, and Wong RO. Immunocytochemical localization of GABA, $GABA_A$ receptors, and synapse-associated proteins in the developing and adult ferret retina. *Vis Neurosci* 14: 1097–1108, 1997.

Katz LC and Shatz CJ. Synaptic activity and the construction of cortical circuits. *Science* 274: 1133–1138, 1996.

Koizumi A, Jakobs TC, and Masland RH. Inward rectifying currents stabilize the membrane potential in dendrites of mouse amacrine cells: patch-clamp recordings and single-cell RT-PCR. *Mol Vis* 10: 328–340, 2004.

Krapf R, Berry CA, and Verkman AS. Estimation of intracellular chloride activity in isolated perfused rabbit proximal convoluted tubules using a fluorescent indicator. *Biophys J* 53: 955–962, 1988.

Leinekugel X, Tseeb V, Ben Ari Y, and Bregestovski P. Synaptic $GABA_A$ activation induces Ca^{2+} rise in pyramidal cells and interneurons from rat neonatal hippocampal slices. *J Physiol* 487: 319–329, 1995.

Lichtman JW and Colman H. Synapse elimination and indelible memory. *Neuron* 25: 269–278, 2000.

Liu J, Morrow AL, Devaud L, Grayson DR, and Lauder JM. $GABA_A$ receptors mediate trophic effects of GABA on embryonic brainstem monoamine neurons in vitro. *J Neurosci* 17: 2420–2428, 1997.

Marandi N, Konnerth A, and Garaschuk O. Two-photon chloride imaging in neurons of brain slices. *Pfluegers* 445: 357–365, 2002.

Marty S, Berninger B, Carroll P, and Thoenen H. GABAergic stimulation regulates the phenotype of hippocampal interneurons through the regulation of brain-derived neurotrophic factor. *Neuron* 16: 565–570, 1996.

Miller RF and Dacheux RF. Intracellular chloride in retinal neurons: measurement and meaning. *Vision Res* 23: 399–411, 1983.

Nakamura T, Kaneko H, and Nishida N. Direct measurement of the chloride concentration in newt olfactory receptors with the fluorescent probe. *Neurosci Lett* 237: 5–8, 1997.

Olney JW. Centripetal sequence of appearance of receptor-bipolar synaptic structures in developing mouse retina. *Nature* 218: 281–282, 1968.

Owens DF, Boyce LH, Davis MB, and Kriegstein AR. Excitatory GABA responses in embryonic and neonatal cortical slices demonstrated by gramicidin perforated-patch recordings and calcium imaging. *J Neurosci* 16: 6414–6423, 1996.

Penn AA, Riquelme PA, Feller MB, and Shatz CJ. Competition in retinogeniculate patterning driven by spontaneous activity. *Science* 279: 2108–2112, 1998.

Penn AA, Wong RO, and Shatz CJ. Neuronal coupling in the developing mammalian retina. *J Neurosci* 14: 3805–3815, 1994.

Redburn DA. Development of GABAergic neurons in the mammalian retina. *Prog Brain Res* 90: 133–147, 1992.

Rothe T, Juttner R, Bahring R, and Grantyn R. Ion conductances related to development of repetitive firing in mouse retinal ganglion neurons in situ. *J Neurobiol* 38: 191–206, 1999.

Sassoè-Pognetto M and Wässle H. Synaptogenesis in the rat retina: subcellular localization of glycine receptors, $GABA_A$ receptors, and the anchoring protein gephyrin. *J Comp Neurol* 381: 158–174, 1997.

Schmid S and Guenther E. Developmental regulation of voltage-activated Na^+ and Ca^{2+} currents in rat retinal ganglion cells. *Neuroreport* 7: 677–681, 1996.

Sernagor E, Young C, and Eglen SJ. Developmental modulation of retinal wave dynamics: shedding light on the GABA saga. *J Neurosci* 23: 7621–7629, 2003.

Shatz CJ and Stryker MP. Prenatal tetrodotoxin infusion blocks segregation of retinogeniculate afferents. *Science* 242: 87–89, 1988.

Sherry DM, Wang MM, Bates J, and Frishman LJ. Expression of vesicular glutamate transporter 1 in the mouse retina reveals temporal ordering in development of rod vs. cone and ON vs. OFF circuits. *J Comp Neurol* 465: 480–498, 2003.

Stacy RC and Wong RO. Developmental relationship between cholinergic amacrine cell processes and ganglion cell dendrites of the mouse retina. *J Comp Neurol* 456: 154–166, 2003.

Syed MM, Lee S, Zheng J, and Zhou ZJ. Stage-dependent dynamics and modulation of spontaneous waves in the developing rabbit retina. *J Physiol* 560: 533–549, 2004.

Thoreson WB and Bryson EJ. Chloride equilibrium potential in salamander cones. *BMC Neurosci* 5:53, 2004.

Thoreson WB, Nitzan R, and Miller RF. Chloride efflux inhibits single calcium channel open probability in vertebrate photoreceptors: chloride

imaging and cell-attached patch-clamp recordings. *Vis Neurosci* 17: 197–206, 2000.

Ueda Y, Iwakabe H, Masu M, Suzuki M, and Nakanishi S. The mGluR6 5′ upstream transgene sequence directs a cell-specific and developmentally regulated expression in retinal rod and ON-type cone bipolar cells. *J Neurosci* 17: 3014–3023, 1997.

Verkman AS. Development and biological applications of chloride-sensitive fluorescent indicators. *Am J Physiol Cell Physiol* 259: C375–C388, 1990.

Vu TQ, Payne JA, and Copenhagen DR. Localization and developmental expression patterns of the neuronal K-Cl cotransporter (KCC2) in the rat retina. *J Neurosci* 20: 1414–1423, 2000.

Wang GY, Olshausen BA, and Chalupa LM. Differential effects of apamin- and charybdotoxin-sensitive K^+ conductances on spontaneous discharge patterns of developing retinal ganglion cells. *J Neurosci* 19: 2609–2618, 1999.

Watanabe S, Koizumi A, Matsunaga S, Stocker JW, and Kaneko A. GABA-mediated inhibition between amacrine cells in the goldfish retina. *J Neurophysiol* 84: 1826–1834, 2000.

Wiesel TN. Postnatal development of the visual cortex and the influence of environment. *Nature* 299: 583–591, 1982.

Wong WT and Wong RO. Changing specificity of neurotransmitter regulation of rapid dendritic remodeling during synaptogenesis. *Nat Neurosci* 4: 351–352, 2001.

Yamada J, Okabe A, Toyoda H, Kilb W, Luhmann HJ, and Fukuda A. Cl^- uptake promoting depolarizing GABA actions in immature rat neocortical neurons is mediated by NKCC1. *J Physiol* 557: 829–841, 2004.

Young TL and Cepko CL. A role for ligand-gated ion channels in rod photoreceptor development. *Neuron* 41: 867–879, 2004.

Yuste R and Katz LC. Control of postsynaptic Ca^{2+} influx in developing neocortex by excitatory and inhibitory neurotransmitters. *Neuron* 6: 333–344, 1991.

Zheng JJ, Lee S, and Zhou ZJ. A developmental switch in the excitability and function of the starburst network in the mammalian retina. *Neuron* 44: 851–864, 2004.

Zhou ZJ. Direct participation of starburst amacrine cells in spontaneous rhythmic activities in the developing mammalian retina. *J Neurosci* 18: 4155–4165, 1998.

Zhou ZJ. A critical role of the strychnine-sensitive glycinergic system in spontaneous retinal waves of the developing rabbit. *J Neurosci* 21: 5158–5168, 2001.